Paneth cell extrusion and release of antimicrobial products is directly controlled by immune cell–derived IFN-γ

Henner F. Farin,[1] Wouter R. Karthaus,[1] Pekka Kujala,[2] Maryam Rakhshandehroo,[3] Gerald Schwank,[1] Robert G.J. Vries,[1] Eric Kalkhoven,[3,4] Edward E.S. Nieuwenhuis,[5] and Hans Clevers[1]

[1]Hubrecht Institute for Developmental Biology and Stem Cell Research and University Medical Centre Utrecht, 3584 CT Utrecht, Netherlands
[2]Antoni van Leeuwenhoek Hospital/Netherlands Cancer Institute, 1066 CX Amsterdam, Netherlands
[3]Section of Metabolic Diseases, Molecular Cancer Research, University Medical Center Utrecht, 3584 CG Utrecht, Netherlands
[4]Netherlands Metabolomics Center, 2333 CC Leiden, Netherlands
[5]Department of Pediatric Gastroenterology, Wilhelmina Children's Hospital, University Medical Center Utrecht, 3584 EA Utrecht, Netherlands

Paneth cells (PCs) are terminally differentiated, highly specialized secretory cells located at the base of the crypts of Lieberkühn in the small intestine. Besides their antimicrobial function, PCs serve as a component of the intestinal stem cell niche. By secreting granules containing bactericidal proteins like defensins/cryptdins and lysozyme, PCs regulate the microbiome of the gut. Here we study the control of PC degranulation in primary epithelial organoids in culture. We show that PC degranulation does not directly occur upon stimulation with microbial antigens or bacteria. In contrast, the pro-inflammatory cytokine Interferon gamma (IFN-γ) induces rapid and complete loss of granules. Using live cell imaging, we show that degranulation is coupled to luminal extrusion and death of PCs. Transfer of supernatants from in vitro stimulated iNKT cells recapitulates degranulation in an IFN-γ–dependent manner. Furthermore, endogenous IFN-γ secretion induced by anti-CD3 antibody injection causes Paneth loss and release of goblet cell mucus. The identification of IFN-γ as a trigger for degranulation and extrusion of PCs establishes a novel effector mechanism by which immune responses may regulate epithelial status and the gut microbiome.

CORRESPONDENCE
Hans Clevers:
h.clevers@hubrecht.eu

Abbreviations used: α-GC, α-galactosylceramide; BAC, bacterial artificial chromosome; Cch, Carbamylcholine; iNKT, invariant Natural Killer T cell; MDP, muramyl dipeptide; ODN, oligodeoxynucleotide; PC, Paneth cell; PGN, peptidoglycan; SN, supernatant; UEA-1, *Ulex europaeus* agglutinin.

Homeostasis of the intestine depends on a complex interplay between the gut microbiota, the intestinal epithelium and immune cells (Duerkop et al., 2009). The epithelium serves as a physical barrier to separate luminal microbes from the body's interior milieu. Innate and adaptive immune responses limit bacterial invasion after barrier dysfunction. Besides its passive role as a physical barrier, the epithelium also actively secretes antimicrobial proteins into the gut lumen (Mukherjee et al., 2008). In the small intestine, Paneth cells (PCs)—highly specialized, terminally differentiated cells located at the bottom of the crypts of Lieberkühn—play a key role by releasing granules containing antimicrobial proteins like lysozyme and α-defensins or cryptdins (Clevers and Bevins, 2013). PCs are long-lived (Ireland et al., 2005) and act as niche cells for intestinal stem cells by providing Wnt, Notch, and EGF signals (Sato et al., 2011a), whereas their maturation depends on Wnt signaling (Van Es et al., 2005; Wehkamp et al., 2007).

The presence of functional PCs is essential for resistance against several enteric bacterial pathogens such as *Salmonella* and *Shigella* (Wilson et al., 1999; Fernandez et al., 2008) and for the maintenance of a normal composition of the gut microbiota (Salzman et al., 2010). Infection with *Toxoplasmosis gondii*, which causes IFN-γ–dependent loss of PCs, results in bacterial

H.F. Farin and W.R. Karthaus contributed equally to this paper.

The Rockefeller University Press $30.00
J. Exp. Med. 2014 Vol. 211 No. 7 1393-1405
www.jem.org/cgi/doi/10.1084/jem.20130753

The Journal of Experimental Medicine

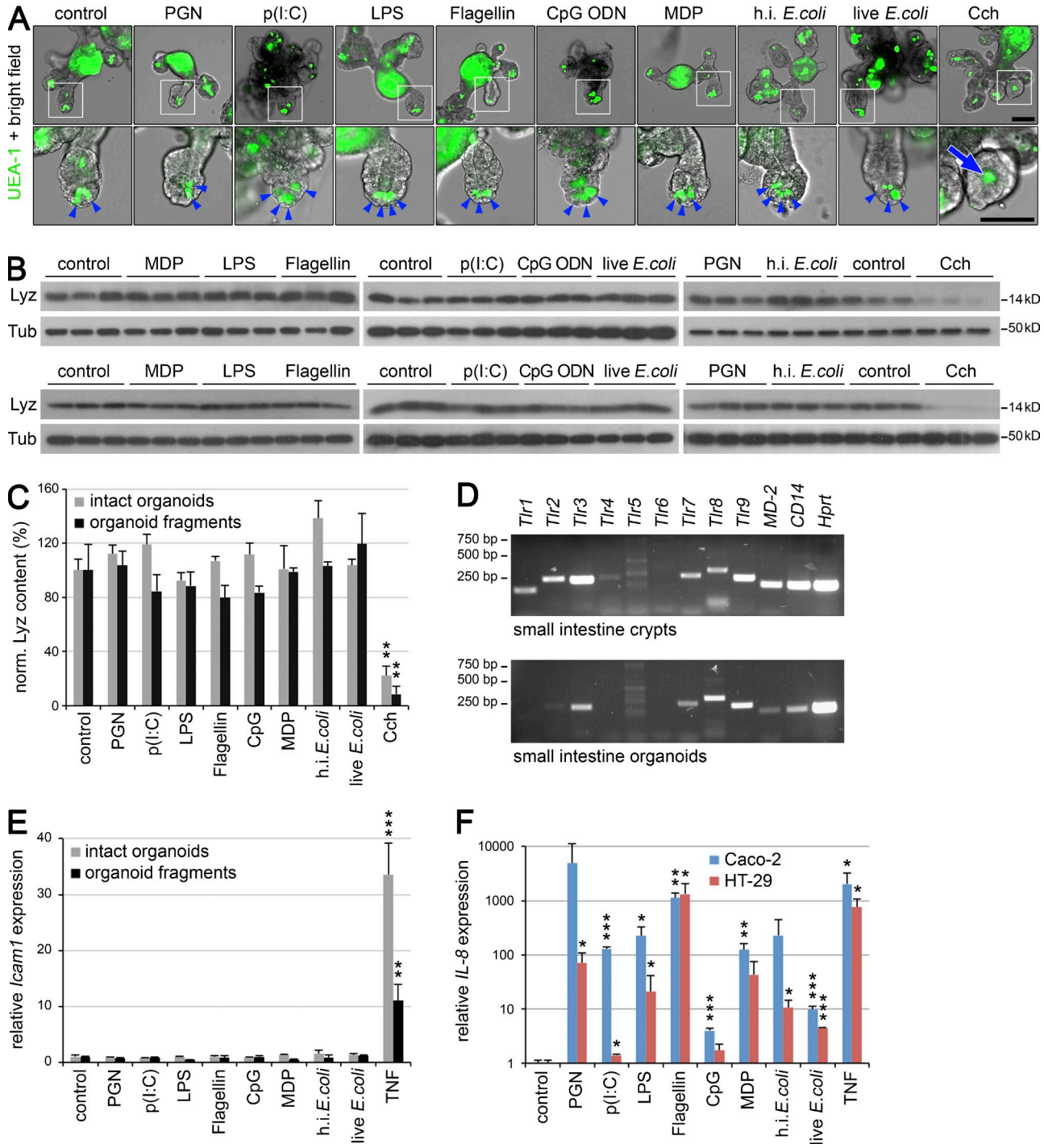

Figure 1. PC degranulation in intestinal epithelial organoids after muscarinergic but not after bacterial stimulation. (A) Small intestinal organoids were stimulated with 10 µg/ml PGN, 100 µg/ml poly(I:C), 1 µg/ml LPS, 0.1 µg/ml flagellin, 1 µg/ml CpG ODN, 100 µg/ml MDP, heat-inactivated (h.i.), or live *E. coli* bacteria or Cch (25 µM) for 12 h, and granules were visualized by UEA-1 lectin staining. Nonstimulated cultures served as controls. PC granules are indicated by blue arrowheads; granule release into the crypt lumen is indicated by the blue arrow. Whole organoids (top) and magnified crypts (bottom) are shown. Bars, 100 µm. (B) Intact organoids in Matrigel (top) were stimulated basolaterally (12 h) or organoid fragments (bottom) were stimulated both apically and basolaterally (2 h), with the indicated bacterial patterns and lysozyme expression assessed by Western blot. Cells were washed to remove luminal lysozyme. α-Tubulin was probed for normalization. Experiments were performed in three parallel cultures. (C) Quantification of lysozyme content from Western Blot data in B. Densitometric analysis of lysozyme signals normalized to α-tubulin expression. Error bars show standard deviation; **, $P < 0.01$; Student's *t* test. Results in A–C were reproduced in two independent experiments. (D) Expression of the indicated microbial pattern receptors; RT-PCR analysis using cDNA from isolated crypts and cultured organoids. *Hprt* was analyzed for normalization. Representative data of three independent

dysbiosis (Raetz et al., 2013). Several gene mutations associated with human Crohn's disease affect PC function (Barrett et al., 2008; Wehkamp and Stange, 2010). Of note, allelic variants of *NOD2* (encoding an intracellular receptor of the bacterial cell wall component muramyl dipeptide [MDP]) are associated with decreased expression of defensins in humans and mice (Wehkamp et al., 2004; Kobayashi et al., 2005). Another risk gene, *ATGL16l1*, encodes a protein involved in autophagy. Mice with hypomorphic *Atgl16l1* mutations show PC defects, which are dependent on simultaneous infection with norovirus (Cadwell et al., 2008; Cadwell et al., 2010). PCs are highly sensitive to endoplasmatic reticulum stress that results from mutations in the transcription factor gene *XBP1* (Kaser et al., 2008), and specific *XBP1* deletion in mouse PCs causes spontaneous ileitis (Adolph et al., 2013).

Given the central role for gut mucosal immunity, it appears crucial to understand the mechanisms that control secretion of antimicrobial proteins and PC turnover. Although granule release into the lumen may occur continuously at a low rate, diverse stimuli are known to trigger collective discharging of PCs (Ayabe et al., 2000). In particular, neurotransmitters that activate muscarinergic acetylcholine receptors are potent inducers of PC degranulation (Satoh et al., 1992). In germ-free mice, recolonization of the intestine by bacteria results in a rapid degranulation that can be completely blocked by muscarinergic antagonists (Satoh, 1988). These observations indicate that acetylcholine-releasing enteric neurons act as a stimulus. On the other hand, PCs respond to bacterial presence in a Myd88/Toll-like receptor (TLR)–dependent fashion (Brandl et al., 2007; Vaishnava et al., 2008). Both oral administration of TLR ligands in vivo (Rumio et al., 2012) and stimulation of isolated murine crypts with bacterial ligands (Ayabe et al., 2000) have been applied in these studies. In addition, acute intestinal damage, e.g., postischemia/reperfusion (Lee et al., 2013) and activation of iNKT cells induce PC degranulation (Nieuwenhuis et al., 2009), suggesting a role for yet unknown immune cell–derived factors.

Clearly, PC degranulation is under complex control, but identification of direct stimuli has been challenged by intrinsic crosstalk between the different tissue compartments in vivo. Here, we have set out to characterize PC degranulation directly using the purely epithelial organoid (minigut) model (Sato et al., 2009). In 3D Matrigel, ever-expanding organoids can be generated from single Lgr5-positive intestinal stem cells using three purified growth factors under serum-free conditions. Organoids form miniguts that recapitulate normal crypt–villus architecture. They consist of a central lumen lined by fully differentiated, highly polarized epithelial cells with their apical brush border facing the lumen. The lumen is surrounded by multiple crypt-like structures containing stem cells, PCs, and transit amplifying daughters. PCs can be readily identified using light microscopy or marker expression, and their presence in each budding crypt is critical because of secretion of niche factors like Wnt3 (Sato et al., 2011a; Farin et al., 2012). Here, we use this cellular model system to address which primary signals can induce PC degranulation. We report a differential sensitivity of PCs for bacterial ligands, cytokines, and muscarinergic stimulation and identify IFN-γ as a potent immune mediator for the release of antimicrobial factors into the gut lumen.

RESULTS

Isolated PCs are refractory to bacterial stimulation

To test if PC degranulation is induced in direct response to bacterial stimulation, we studied the effect of microbial antigens added to the culture medium of small intestinal organoids. 12 h after addition of peptidoglycan (PGN), poly(I:C), LPS, flagellin, CpG oligodeoxynucleotides (ODNs), MDP, and heat-inactivated or live *E. coli* bacteria PC granules were visualized using UEA-1 (*Ulex europaeus* agglutinin 1) lectin staining (Fig. 1 A). We observed no change in organoid morphology and no effect on PC granules under all conditions tested. As a positive control, cholinergic stimulation with Carbamylcholine (Cch) caused complete loss of epithelial granules, demonstrating the physiological competence of cultured PCs similar to their counterparts in vivo (Satoh et al., 1992). The absence of any PC secretory response to bacterial stimuli was confirmed by Western blot analysis of lysozyme content in organoids that were mechanically sheared and extensively washed to separate the pool of intracellular lysozyme from the pool that had been secreted into the crypt lumen (Fig. 1, B and C).

Addition of the various agents to intact organoids results in basolateral exposure to bacterial antigens, similar to disruption of the epithelial barrier in vivo. We next explored the effects of exposure on both the apical and basal sites. For this, we generated organoid fragments by mechanical shearing. These were resuspended in culture medium containing the panel of bacterial agents. Lysozyme content was quantified after 2 h at 37°C—an experimental setting analogous to the stimulation of freshly isolated crypts used previously (Ayabe et al., 2000). No significant decrease of the epithelial lysozyme content was measured for any of the bacterial stimuli, whereas controls using Cch again resulted a complete discharge of PCs (Fig. 1, B and C). We concluded that bacterial stimulation from both basolateral and apical epithelial sides represents no direct trigger for PC degranulation in our system.

By RT-PCR analysis, we found that the expression of microbial pattern receptors (*Tlr2*,*3*,*7*,*8*,*9*, *MD-2* and *Cd14*) is

experiments. (E) Intact organoids and organoid fragments were stimulated with the indicated stimuli for 1 h, and *Icam1* expression was assessed by qPCR analysis. Mean relative expression ± SD in $n = 3$ parallel wells; **, $P < 0.01$; ***, $P < 0.001$; Student's *t* test. Data representative of three independent experiments. (F) Human colon cancer cell lines Caco-2 and HT-29 were stimulated with the indicated stimuli for 1 h, and *IL-8* expression was assessed by qPCR. Mean relative expression ± SD (log_{10} scale) in $n = 3$ parallel wells; *, $P < 0.05$; **, $P < 0.01$; ***, $P < 0.001$; Student's *t* test. Experiment has been performed twice.

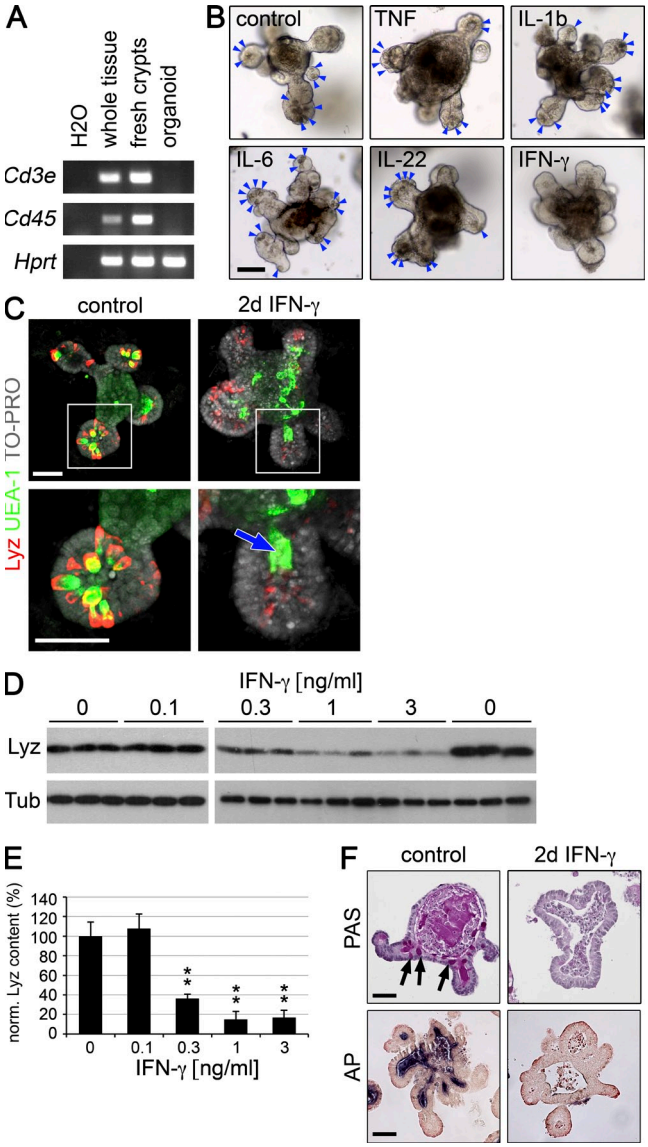

Figure 2. IFN-γ–induced PC degranulation. (A) RT-PCR expression analysis of *Cd3e* (T cells) and *Cd45* (leukocytes) in whole mouse small intestinal RNA or in RNA from freshly isolated crypts and cultured organoids. *Hprt* expression was used for normalization. Representative results of 2 independent experiments. (B) Morphology of small intestinal organoids 2 d after addition of mouse recombinant TNF, IL-1b, IL-6, IL-22 (all at 20 ng/ml) or IFN-γ (5 ng/ml) to the culture medium. PCs were observed in all cultures (blue arrowheads) except after IFN-γ treatment. Representative images from three independent experiments. (C) Small intestinal organoids were stimulated with IFN-γ (2 d; 5 ng/ml) followed by lysozyme immunostaining (red) and UEA-1 lectin staining (green). Blue arrow shows accumulation of UEA-1$^+$ mucus in the crypt lumen. 3D projected confocal images show nuclei (gray) stained with TO-PRO3. Representative images from two independent experiments. (D) Organoids were stimulated for 2 d with indicated concentrations of IFN-γ and epithelial lysozyme content was analyzed by Western blot; results are representative for two independent experiments. (E) Quantification of Western blot data in D by densitometric analysis. Mean normalized lysozyme signal ± SD of triplicate wells is shown; **, $P < 0.01$; Student's *t* test. (F) Histological analysis of organoids 2 d after addition of 5 ng/ml IFN-γ by PAS and alkaline phosphatase (AP) staining. Black arrows show loss of mucus-filled goblet cells. Images are representative from two independent experiments. Bars, 50 µm.

maintained in organoids compared with freshly isolated crypts (Fig. 1 D), arguing against nonresponsiveness due to transcriptional down-regulation. We used quantitative RT-PCR analysis to study if microbial stimuli can cause transcriptional activation of NF-κB signaling. Despite expression of cognate receptors (Tlr2, 3, and 9 for PGN, poly(I:C), and CpG ODN, respectively) stimulation in organoids did not induce expression of *Icam1* or other NF-κB targets (Fig. 1 E and not depicted). TNF stimulation did cause marked *Icam1* induction, suggesting that upstream events in TLR signaling mediate refractoriness to bacterial stimuli. As a positive control, human colon cancer cell lines (Caco-2 and HT-29) strongly responded to all microbial stimuli by induction of *IL-8* expression (Fig. 1 F).

A direct role for IFN-γ in loss of PC granules

We hypothesized that PC degranulation as observed in freshly isolated intestinal crypts (Ayabe et al., 2000) might depend on bacterial sensing by co-isolated leukocytes. Using RT-PCR analysis, we indeed found that *Cd3e*- and *Cd45*-expressing immune cells were present in primary crypt preparations, but not in established organoid cultures (Fig. 2 A). We subsequently aimed to identify immune cell mediators that might indirectly cause PC degranulation after bacterial stimulation by testing the activity of several (proinflammatory) cytokines. PCs were morphologically unaffected in the presence of recombinant TNF, IL-1b, IL-6, or IL-22 (all at 20 ng/ml; 2 d; Fig. 2 B). In contrast, treatment with recombinant IFN-γ caused complete loss of PC granules as indicated by morphology, lysozyme immunostaining, and measurement of epithelial lysozyme content (Fig. 2, B–D). The minimal effective concentration of recombinant IFN-γ was 0.3 ng/ml (Fig. 2 E). Histologically, IFN-γ–treated organoids were characterized by a loss of mucus-containing goblet cells (Periodic acid-Schiff [PAS] staining) and mature enterocytes (as observed by alkaline phosphatase [AP] staining; Fig. 2 F), demonstrating a direct effect of this cytokine on other differentiated cell lineages as well.

Release of granules coincides with induction of apoptosis and PC loss

Recent experiments have shown that prolonged IFN-γ exposure in vivo during *T. gondii* infection results in a complex intestinal pathology that is characterized but also caused by the loss of PCs (Raetz et al., 2013). However, the kinetics and directness of the epithelial response to IFN-γ have not yet been studied. Long-term exposure during several organoid passages caused successive and dose-dependent reduction in organoid number (Fig. 3 A). Time course experiments showed a strong apoptotic response starting 16 h after addition of 1 ng/ml IFN-γ as measured by FACS analysis of cleaved Caspase3 staining (Fig. 3, A and B). Significant reduction of the epithelial lysozyme content was detected on Western blot

after a similar incubation period (Fig. 3 C). qPCR analysis of marker gene expression in PCs (*Lyz1* and *Defa6*) and stem cells (*Lgr5* and *Olfm4*) showed progressive reduction to <20% of control levels after 24 h of treatment, whereas the IFN-γ target gene *Irf1* was stably induced (Fig. 3 D). These results indicate that IFN-γ affects epithelial homeostasis by induction of programmed cell death, which may contribute to PC loss. To test if PCs are maintained after degranulation, we performed in situ hybridization of *Defa6* mRNA and anti-CD24 immunostainings (Sato et al., 2011a) to label their cytoplasm and membranes, respectively (Fig. 3, E and F). Reduced presence of PCs was found and FACS quantification showed that ∼25% of $CD24^+$ cells were left after 5 d of treatment (Fig. 3 G and Fig. S1 B). Ubiquitous induction of the IFN-γ target MHC2, suggested a direct effect on all cell types, including PCs (Fig. 3 E). 4 d after withdrawal of IFN-γ from the culture medium, the organoid morphology had normalized and granules had recovered (Fig. 3 H), demonstrating that the epithelium can restore either by recharging of granules or by de novo generation of PCs.

IFN-γ triggers rapid release of granules and epithelial extrusion of PCs

To study the mechanism and the consequences of degranulation at a single-cell level, we performed time-lapse imaging. PC granules were labeled with ZP-1, a fluorescent and membrane permeable Zn^{2+} chelator (Giblin et al., 2006). Organoid morphology and marker distribution were followed after IFN-γ addition using confocal microscopy (Fig. 4 A and Videos 1–3). We found that degranulation was not synchronous

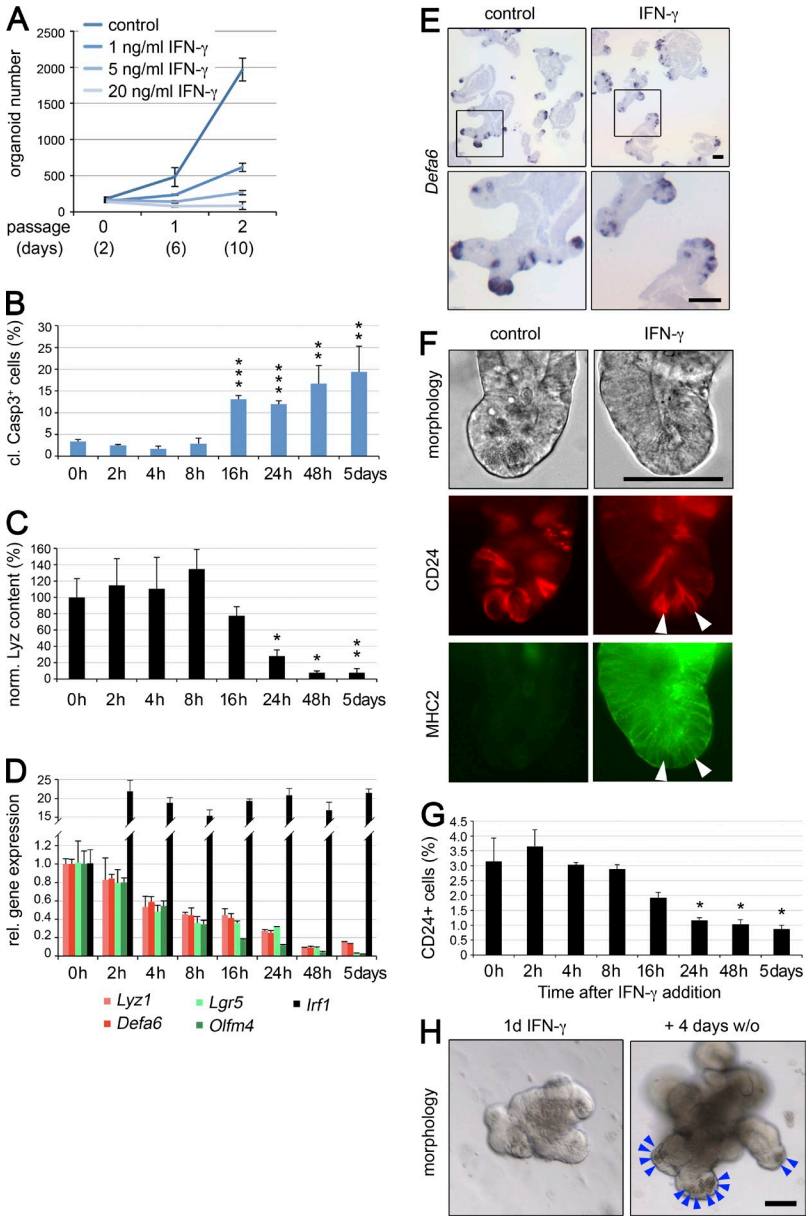

Figure 3. Reduced organoid growth and progressive loss of PCs after IFN-γ exposure. (A) Organoid number after prolonged culture in presence of indicated concentrations of IFN-γ. Mean of $n = 3$ independent cultures ± SD is shown, experiment was performed once. All concentrations caused a significantly reduced growth compared with controls (passage 1, $P < 0.05$; passage 2, $P < 0.001$, as determined by Student's *t* test). (B–D) Time-course analysis of organoids stimulated with 1 ng/ml IFN-γ for the indicated times. (B) Dissociated organoid cells were analyzed by FACS after cleaved Caspase-3 staining. Mean percentage of positive cells from $n = 3$ independent experiments ± SD is shown; **, $P < 10^{-2}$; ***, $P < 10^{-4}$; Student's *t* test. See Fig. S1 A for original FACS data. (C) Quantification of epithelial lysozyme content by Western blot. Experiment was performed in $n = 3$ parallel cultures; mean normalized signals ± SD are shown; *, $P < 0.05$; **, $P < 0.01$; Student's *t* test. Results were reproduced twice independently. (D) qPCR analysis for marker gene expression of PCs (*Lyz1*, *Defa6*), stem cells (*Lgr5*, *Olfm4*) and the IFN-γ target gene *Irf1*. Mean normalized expression values ($n = 3$ parallel cultures ± SD) are shown. Results are representative for two independent experiments. (E) In situ hybridization analysis of *Defa6* expression after IFN-γ treatment (5 ng/ml for 2 d). Overview (top) and magnified images (bottom) are shown that are representative for 3 independent experiments. (F) Immunostaining of membrane markers: CD24 on PCs (red) and the IFN-γ target MHC2 (green) after IFN-γ stimulation (1 d, 1 ng/ml). Note the ubiquitous MHC2 induction also on degranulated PCs (white arrowheads). Images are representative for two independent experiments. (G) Organoids were stimulated for the indicated times (1 ng/ml IFN-γ) before quantification of CD24-positive cells by FACS. Mean cell number (of $n = 2$ independent experiments ± SD) is shown. *, $P < 0.05$ as determined by Student's *t* test. See Fig. S1 B for the original FACS data. (H) Morphology 1 d after treatment with 5 ng/ml IFN-γ and subsequent culture for 4 d in normal medium. Blue arrowheads show reformation of PC granules. Bars, 50 µm. Experiment was repeated three times.

within a given crypt. Individual PCs extruded their fluorescent label in an all-or-nothing manner, rather than through continuous exocytosis of vesicles. At a cellular level this process was completed within minutes. Between organoids, the onset and completion of degranulation was variable, but was clearly dependent on the IFN-γ concentration (6–12 h at 5 ng/ml and 4–8 h with 20 ng/ml IFN-γ).

Transmission electron microscopy also showed collective extrusion of PC granules (Fig. 4 B). Generation of large apical vacuoles was observed, reminiscent of the ultrastructural changes after muscarinergic stimulation in vivo (Satoh et al., 1992). After secretion into the crypt lumen, the electron-dense granules dissolved and the ZP-1 fluorescent signal rapidly dispersed (Fig. 4, A and B; and Videos 2 and 3). In other cases, granules remained densely packed, indicating the release of large PC fragments (Fig. 4 B). We found no indication of PC mitochondrial damage like that observed by electron microscopy after IFN-γ exposure during *T. gondii* infection (Raetz et al., 2013). After 12 h in the presence of 20 ng/ml IFN-γ, mature PC granules were absent, but we detected cells containing small electron-dense granules that may correspond to discharged or newly differentiating PCs.

To analyze PC fate and turnover after IFN-γ stimulation, we generated live cell reporters to trace granules and nuclei simultaneously. Granules were visualized by expression of a Lyz2-RFP fusion protein that was inserted in the *Lyz2* genomic region in bacterial artificial chromosome (BAC) transgenic organoids (Schwank et al., 2013). Nuclei were fluorescently

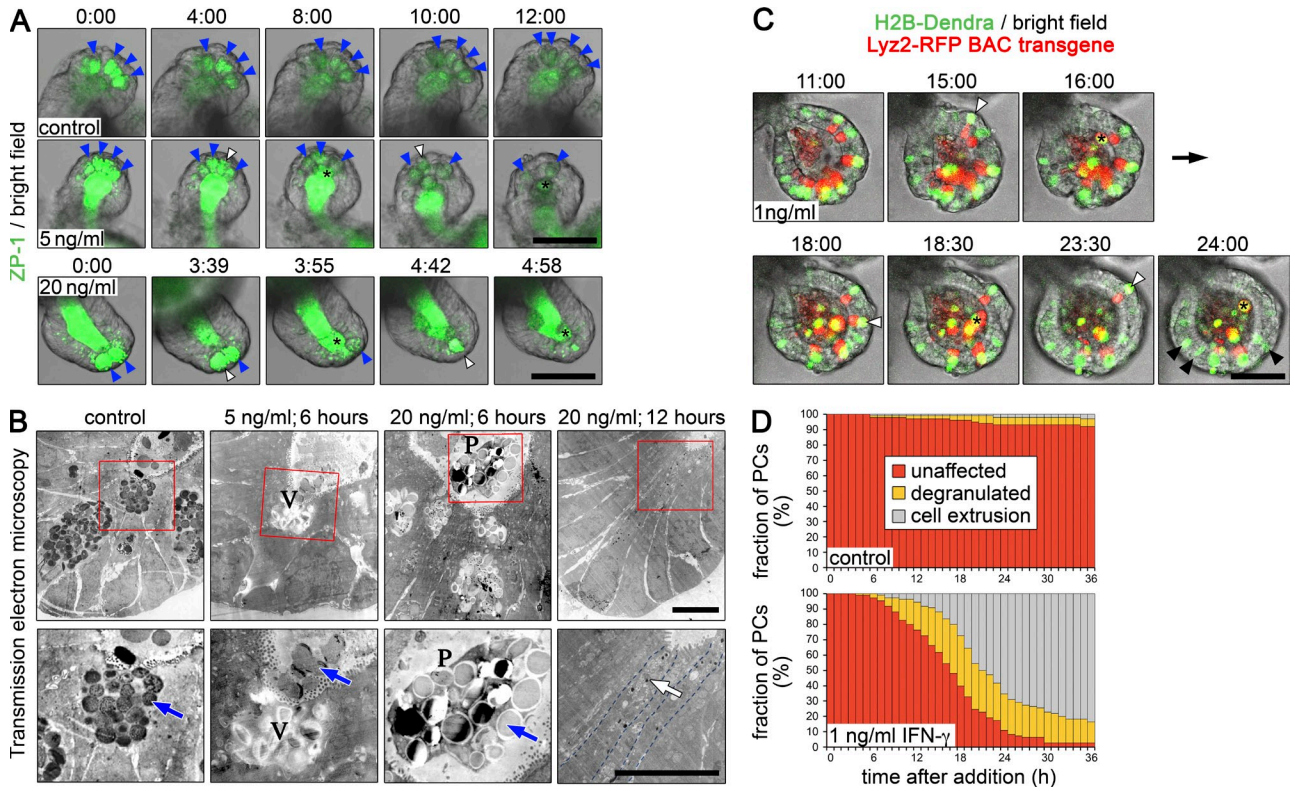

Figure 4. IFN-γ induces rapid granule release that is caused by PC extrusion. (A) Time-lapse analysis of PC degranulation. Granules were labeled with the fluorescent Zn^{2+} chelator ZP-1, followed by live microscopy (still images of Videos 1–3). Untreated controls (top row) or cultures stimulated with 5 ng/ml (middle row) or 20 ng/ml IFN-γ (bottom row). Time after addition of IFN-γ is indicated on top (hours:min). Blue arrowheads show unaffected PCs; white arrowheads mark PCs that release their granules during the next time interval, as labeled by asterisks. Note that the fluorescent signal decreases due to bleaching. Experiment was repeated twice with at least 5 organoids per condition. Bars, 50 µm. (B) Transmission electron microscopy analysis of control organoids (left) and cultures stimulated with IFN-γ for 6 h (middle) or 12 h (right). Magnified regions (red boxes) are shown in the bottom row. Blue arrows mark PC granules; residual small granules are marked with a white arrow. The label V shows a large apical vacuole; P marks extruded cell fragments with densely packed granules; cell membranes are marked with dashed lines. Representative images from 1 experiment with $n > 10$ organoids analyzed per condition. Bars, 5 µm. (C) Cell-fate analysis of PCs after degranulation using live reporters (still images of Video 4). BAC transgenic organoids expressing Lyz2-RFP in PC granules (red signal) and lentiviral Histone 2B (H2B)-Dendra in nuclei (green signal). Time after addition of 1 ng/ml IFN-γ is indicated on top (hours:min). White arrowheads mark individual PCs that extrude both granules and cell nucleus during the next time interval (asterisks). After 24 h the epithelium is devoid of Lyz2-RFP and only few labeled nuclei remain (black arrowheads). Note that long-lived PCs accumulate H2B-Dendra. Results were reproduced in two independent experiments. (D) Quantification of PC fate from time-lapse data in C. In untreated control cultures (top) and after treatment (1 ng/ml IFN-γ; bottom), the status of >100 PCs each was tracked for 36 h. PCs were scored as unaffected (red bars), and then degranulated with nucleus present (orange bars) or extruded (gray bars).

labeled by lentiviral expression of Histone 2B-Dendra (H2B-Dendra). We took advantage of the fact that ubiquitous expression driven by the CMV promoter resulted in strongest nuclear fluorescence in post-mitotic PCs that most likely accumulated the label. Strikingly, confocal microscopy showed that IFN-γ treated PCs co-released their nucleus together with their granules into the crypt lumen (Fig. 4 C and Video 4). Tracking of individual PCs ($n > 100$) showed that the majority of degranulation events resulted in this outcome with only 18% of all PC nuclei remaining after 36 h (1 ng/ml IFN-γ), while control cultures showed only infrequent spontaneous degranulation (Fig. 4 D and Video 5). Our results demonstrate that IFN-γ signaling mobilizes the entire epithelial pool of antimicrobial products by induction of PC extrusion. We conclude that epithelial recovery occurs by de novo differentiation rather than by recharging of PCs.

IFN-γ–mediated granule release in response to iNKT cell stimulation

Next, we studied if endogenous cytokine levels produced by stimulated leukocytes are sufficient to induce PC release. We used the mouse invariant natural killer T (iNKT) hybridoma line DN32.D3, which secretes IFN-γ and other immune mediators upon CD1D-antigen presentation of the lipid antigen α-galactosylceramide (α-GC; Bialecki et al., 2009; Nieuwenhuis et al., 2009). Conditioned cell culture supernatants (SNs) were generated from control iNKT cells and after α-GC stimulation in the presence or absence of CD1D-expressing HeLa cells. These SNs were transferred to organoids (see scheme in Fig. 5 A). iNKT cell stimulation caused pronounced secretion of IFN-γ as observed by ELISA (Fig. 5 B). 2 d after addition to organoids, PC degranulation was analyzed using UEA-1 lectin staining and Western blot quantification of epithelial lysozyme. We found a loss of granules that was dependent on antigen presentation to iNKT cells, whereas direct α-GC stimulation of organoids had no effect (Fig. 5, C–E). Pretreatment with a neutralizing anti–IFN-γ antibody efficiently blocked activity in SNs from activated iNKT cells and also neutralized the effect of recombinant IFN-γ (Fig. 5 F). These results show that IFN-γ (produced at endogenous levels after stimulation) represents the main soluble trigger of PC release from iNKT cells.

IFN-γ acts as a potent intestinal secretagogue after T cell activation in vivo

Acute T cell stimulation using anti-CD3 antibody injection in vivo causes a severe but transient intestinal pathology that is characterized by epithelial apoptosis and massive villus blunting (Merger et al., 2002; Miura et al., 2005). However, it is unclear which of these effects can be attributed to IFN-γ and whether PC granules are released upon immune activation in vivo. We addressed these questions by i.p. injection of anti-CD3 in C57BL/6 wild-type and *IFN*-γ knock out (KO) mice. Intestines were collected for lysozyme immunohistochemistry 24 h later. In wild-type mice, anti-CD3 injection caused marked reduction of the number of lysozyme-positive PCs as counted per crypt section (Fig. 6, A and B). This confirmed our in vitro observation that PC granules are rapidly mobilized after immune stimulation. This effect was highly significant and strongest in the proximal intestine (duodenum) where the number of stained PCs was reduced by half ($n = 7$; $P < 10^{-6}$). In homozygous *IFN*-γ KO mice, however, lysozyme-positive PCs were maintained in all regions of the intestine, demonstrating that IFN-γ is specifically required for granule loss. In situ hybridization for *Defa6* mRNA as a cytoplasmic marker of PCs showed a similar response (Fig. 6, C and D), suggesting loss of entire PCs, as observed in vitro. T cell activation stimulated apoptosis broadly in the epithelium as observed by cleaved Caspase-3 immunostaining (Fig. 6, E–G). Importantly, the number of apoptotic cells was unaffected in *IFN*-γ KO intestines, demonstrating that PC rescue in this genotype is not a general result of an attenuated inflammatory reaction. Villus damage was most apparent in distal regions of the intestine (ileum) and clearly ameliorated in *IFN*-γ KO mice (Fig. 7 A). Here, PAS staining showed an IFN-γ–dependent release of goblet cell mucus that also massively occured in the colonic epithelium. In colon organoids, extrusion of goblet cell mucus after IFN-γ treatment was recapitulated (Fig. 7 B), demonstrating a more general role of this cytokine as a direct intestinal secretagogue for both Paneth and goblet cells.

DISCUSSION

Gut mucosal immunity is controlled by complex interactions among epithelium, microbiota, and the immune system, which complicates the dissection of signaling mechanisms. Here, we have used purely epithelial cultures to show that release of antimicrobial peptides and PC turnover are directly controlled by immune signals. IFN-γ was identified as the main mediator of PC degranulation after CD1D-dependent stimulation of iNKT cells (Nieuwenhuis et al., 2009) and after anti-CD3 stimulation of T cells in vivo. We propose that the proinflammatory cytokine may represent a danger signal to induce PC release and to react to microbial challenges. The exact cellular source of IFN-γ − most likely − depends on the physiological situation. Besides systemic IFN-γ release such as upon α-GC stimulation of iNKT cells (Nieuwenhuis et al., 2002), activation of intra-epithelial lymphocytes could also represent a paracrine source of IFN-γ (Guy-Grand et al., 1998; Cheroutre et al., 2011).

Organoid cultures have allowed us to visualize the rapid and complete discharging of PCs by IFN-γ or by muscarinergic stimulation, but cultured PCs were insensitive to a broad spectrum of microbe-associated molecular patterns, which contrasts with previous data obtained using freshly isolated crypts (Ayabe et al., 2000). While evidence suggests that microbial patterns can directly trigger PC function in vivo (Rumio et al., 2012; Brandl et al., 2007; Vaishnava et al., 2008), lack of *Tlr4* expression in PCs (Tanabe et al., 2005) indicates an indirect nature of the effect seen after stimulation of primary crypts LPS. Also, the fact that degranulation after bacterial inoculation of germ-free mice can be inhibited by atropine

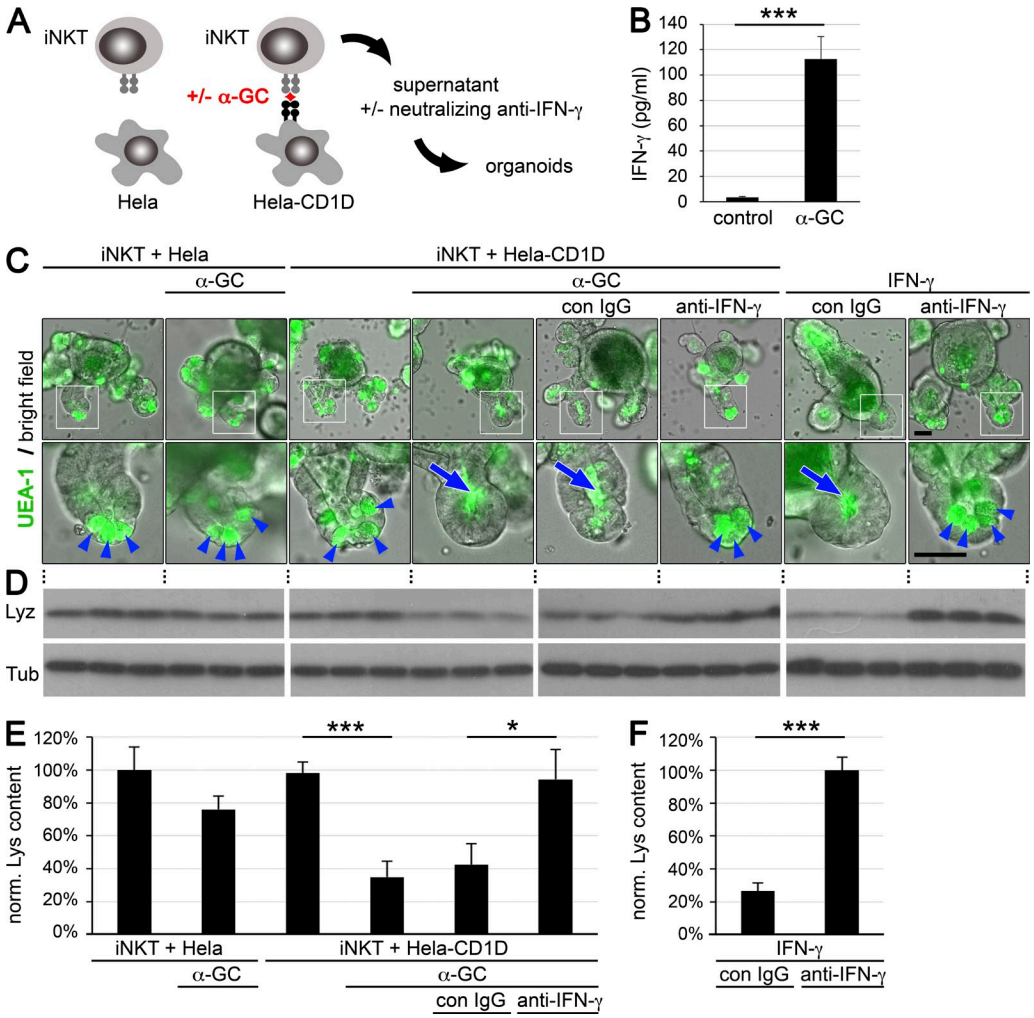

Figure 5. Lipid antigen stimulation of iNKT cells triggers PC degranulation in an IFN-γ–dependent manner. (A) Experimental strategy. Cell culture SNs were collected from activated iNKT cells and transferred to the culture medium of small intestinal organoids. iNKT activation in the presence of the lipid antigen α-GC and HeLa-CD1D antigen presentation. SNs were preincubated with neutralizing anti–IFN-γ antibody or control IgG. (B) ELISA quantification of IFN-γ levels in SNs of control iNKT cells and after α-GC stimulation (both in presence of HeLa-CD1D cells). Means of quadruplicate measurement is shown (±SD; ***, $P < 10^{-4}$; Student's *t* test). (C) Small intestinal organoids were cultured for 2 d in presence of iNKT SNs, followed by UEA-1 lectin staining; blue arrowheads label unaffected PCs and blue arrows show discharged PCs. Bars, 100 µm. (D) Western blot analysis of epithelial lysozyme content; conditions as in C. Organoid lysates from three parallel cultures; α-tubulin was probed for normalization. (E and F) Quantification of lysozyme expression from Western blot data shown in D by densitometric analysis. Mean normalized signals ± SD are shown; *, $P < 0.05$; ***, $P < 0.001$; Student's *t* test. Data (B–F) are from one representative experiment of two independent experiments.

favors an indirect mechanism, such as involvement of acetylcholine-secreting enteric neurons (Satoh, 1988). Interestingly, bacterial colonization is required for PC loss after *T. gondii* infection (Raetz et al., 2013). Here, however, bacterial sensing (and Myd88 expression) by T cells was required, demonstrating that continuous immune stimuli act on PCs in this model. Future research will benefit from the use of organoid cultures to identify mechanisms that regulate endotoxin tolerance of intestinal epithelial cells, which has been noted previously (Lotz et al., 2006). Given the broad distribution of bacterial antigens within the gut lumen, nonresponsiveness to microbial patterns (as observed by us) could be beneficial to avoid continuous stimulation by commensals.

Our study shows that organoids are a useful model to address PC function because analysis of pure epithelium prevents indirect effects of co-isolated (intraepithelial) leukocytes that are unavoidable in primary material, and organoids, even ex-Matrigel, are less fragile than fresh crypts—the latter degenerate instantly after isolation and allow short stimulations only. Thus, organoids offer a more sensitive system because full PC discharging can be achieved, whereas maximal secretion using fresh tissue never exceeds >20–30% under the conditions used (Ayabe et al., 2000). In addition, live imaging offers the unique possibility to follow cellular mechanisms and consequences upon degranulation.

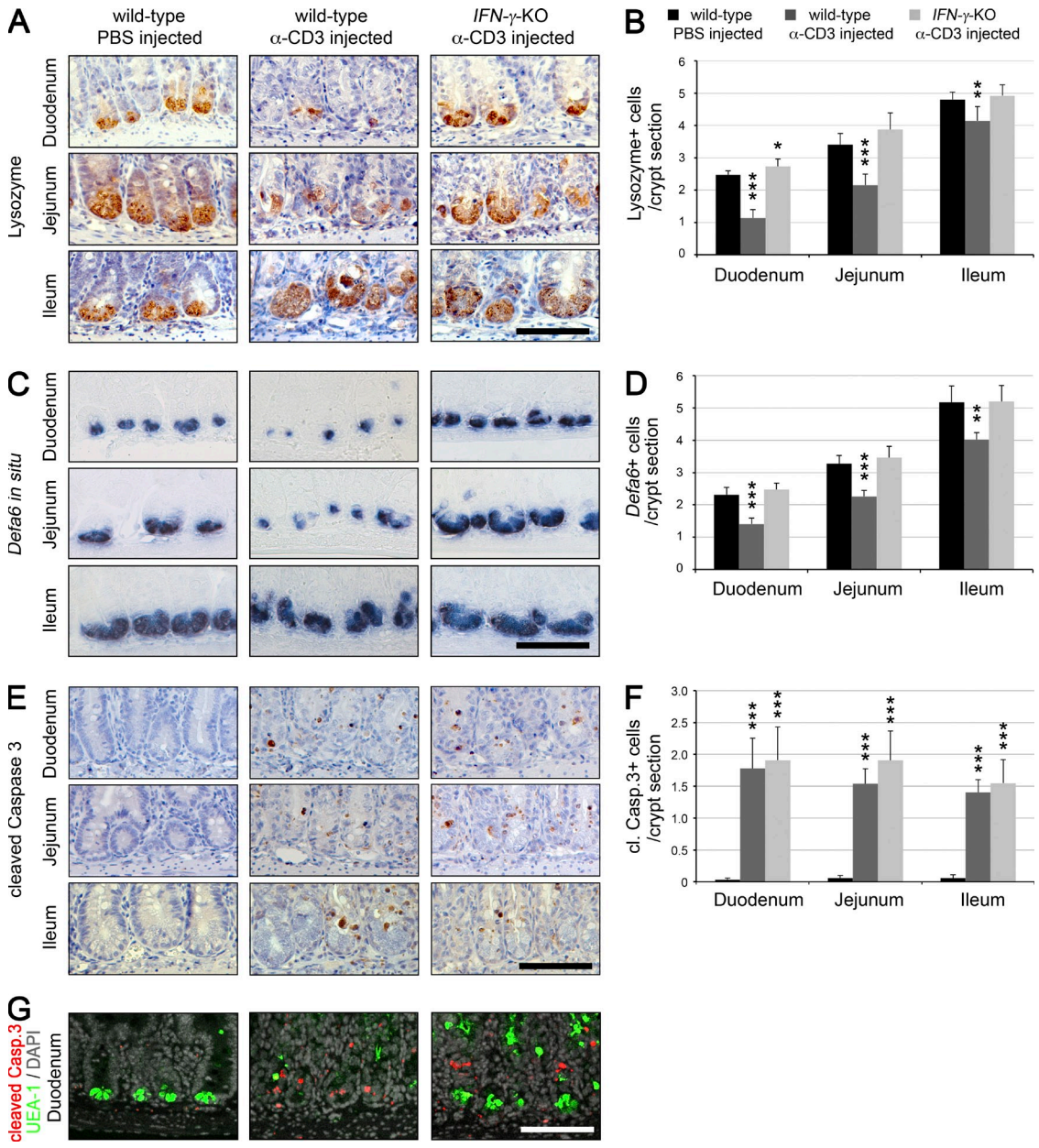

Figure 6. T cell activation in vivo causes IFN-γ dependent Paneth loss. (A–G) Wild-type and *IFN-γ* KO mice were injected i.p. with anti-CD3 antibody (50 µg/mouse); as a control PBS was injected in wild-type mice. 24 h after injection, mice were sacrificed for histological analysis. Groups of $n = 7$ animals per condition were used and results were reproduced in 2 independent experiments. (A) Lysozyme immunostaining shows reduced PC granules after T cell activation in wild-type but not in *IFN-γ* KO mice. (B) Quantification of lysozyme-positive cells per crypt section in 45 crypts/animal/region. Mean number ± SD is shown. *, $P < 0.05$; **, $P < 0.01$; ***, $P < 10^{-4}$; Student's *t* test compared with control-injected mice. (C) *Defa6* in situ hybridization. (D) Quantification of *Defa6*$^+$ cells per crypt section; mean cell number ± SD is shown. **, $P < 10^{-3}$; ***, $P < 10^{-5}$; Student's *t* test compared with control-injected mice. (E) Cleaved Caspase-3 immunostaining shows pronounced induction of apoptosis in both wild-type and *IFN-γ* KO crypts. (F) Quantification of cleaved Caspase-3$^+$ cells per crypt section. Mean cell number ± SD is shown. ***, $P < 10^{-6}$; Student's *t* test compared with control-injected mice. (G) Co-staining of cleaved Caspase-3 (red) and PC granules (UAE-1; green) shows broad induction of apoptosis, also in non-PCs. Nuclei stained with DAPI (gray). Bars, 50 µm.

We found that IFN-γ acts as a potent intestinal secretagogue both on Paneth and goblet cells. Goblet cell mucus serves as matrix to retain and concentrate antimicrobial PC products (Meyer-Hoffert et al., 2008). Given that T cell activation can cause severe damage to the intestine, such as apoptosis and disruption of the intestinal barrier (Merger et al., 2002; Miura et al., 2005), this massive release of antimicrobial factors might help to limit bacterial entry. Extrusion of PCs has been noted previously upon induction of ER stress or perturbation of zinc ion homeostasis (Sawada et al., 1991; Zhao

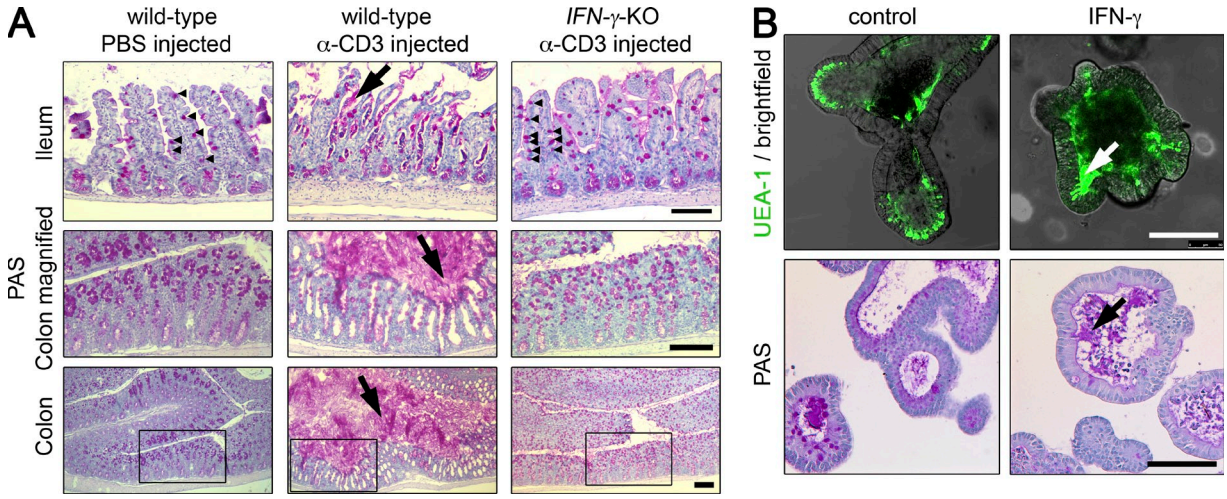

Figure 7. IFN-γ acts as potent secretagogue of goblet cell mucus. (A) PAS staining on histological sections of anti-CD3–injected mice (same experiment as in Figure 6). Black arrows show massive extrusion of goblet cell mucus in wild-type but not in *IFN-γ* KO mice. Black arrowheads mark unaffected goblet cells on ileal villus (top row); note the IFN-γ–dependent villus damage. For the colon magnified regions (middle row) and overview images (bottom row) are shown. Phenotypes were fully penetrant in $n = 7$ animals per group and results were reproduced in 2 independent experiments. (B) Mouse colon organoids were treated with IFN-γ for 24 h (5 ng/ml) and stained with UEA-1 lectin (top) or PAS (bottom). Images are representative of two independent experiments. Arrows label secretion of goblet cell mucus. Bars, 100 µm.

et al., 2010; Grootjans et al., 2011; Adolph et al., 2013). Coextruded genomic DNA might serve as a clot to seal crypts or act as a scaffold to trap bacteria, analogous to extracellular DNA webs that are released by cell death from activated neutrophils (Brinkmann et al., 2004). It should be noted that human Defensin 6 (HD6) itself can form nanonets to trap bacteria (Chu et al., 2012). Although mice lack a functional HD6 homologue, it has been reported that defensins have DNA-binding activity (Tewary et al., 2013) and might associate with released PC DNA. After elimination of PCs, new PCs can rapidly be generated de novo from adjacent stem cells as early as 12–24 h after challenge (Sawada et al., 1991). Continuous IFN-γ stimulation did not cause desensitization but a progressive loss of PCs. This occurred at concentrations comparable to IFN-γ serum levels reported in common mouse inflammatory bowel disease (IBD) models (Alex et al., 2009), arguing for a direct effect on PCs in chronic pathologies such as persistent murine norovirus infection in *Atg16L1* mice or toxoplasmosis (Cadwell et al., 2010; Raetz et al., 2013). Future studies should address if PC dysfunction and associated changes of the gut flora are causally involved in other IFN-γ–driven IBD models (Kontoyiannis et al., 2002; Saha et al., 2010). Our observations might explain the reduction of PC numbers observed in other IFN-γ–dependent pathologies such as graft versus host disease and celiac disease (Nilsen et al., 1998; Di Sabatino et al., 2008; Eriguchi et al., 2012; Levine et al., 2013). Possibly the PC status might serve as sensitive reporter for IFN-γ signaling in clinical biopsies.

Given that organoid cultures can be established from human biopsies (Sato et al., 2011b), the phenotypic characterization of PC function in vitro may provide an important diagnostic tool to dissect disease mechanisms in these patients. The pharmacologic modulation of IFN-γ signaling to control PC function and survival may allow a new strategy to modify host defense.

MATERIALS AND METHODS

Organoid culture. Small intestinal organoids were established from wild-type C57BL/6 mice, cultured as described previously (Sato et al., 2009; Farin et al., 2012) and passaged weekly at a 1:6 split ratio. Organoids were stimulated for the indicated times by addition of recombinant murine IFN-γ (1 to 20 ng/ml; R&D Systems), mTNF-α (PeproTech), mIL-1b (Sigma-Aldrich), mIL-6 (eBioscience), mIL-22 (R&D Systems; all at 20 ng/ml) or Cch (25 µM; Sigma-Aldrich). Microbial stimuli were PGN (10 µg/ml; InvivoGen from *S. aureus*), p(I:C) (100 µg/ml; InvivoGen), LPS (1 µg/ml; Sigma-Aldrich from *E. coli* 026:B7), flagellin (0.1 µg/ml; InvivoGen from *S. typhimurium*), CpG ODN 1668 (1 µg/ml; Enzo), and MDP (100 µg/ml; InvivoGen). Log phase *E. coli* bacteria (strain K-12) were washed and added to the culture medium directly (in absence of penicillin/streptomycin), or after heat inactivation for 10 min at 95°C; per epithelial cell 100 bacteria were added. Mouse colon organoids were cultured as described previously for human colon cultures (Sato et al., 2011b). Colon organoids were differentiated toward goblet cells by addition of γ-secretase inhibitor DAPT (10 µM; Sigma-Aldrich) for 5 d before IFN-γ treatment. For stimulation of fragmented epithelia, organoids were collected in cold medium and mechanically sheared using glass Pasteur pipettes. Dispersal of crypts was confirmed by light microscopy and 100 crypts each were stimulated at 37°C, 5% CO_2.

BAC transgenesis of organoids has been described recently (Schwank et al., 2013), in brief a tagRFP-PGK::neo-cassette was inserted before the STOP codon of the mouse *Lys2* locus (ENSMUSG00000069516) using BAC clone RP11-1105J23. BAC DNA was transfected in organoid cells using Lipofectamine 2000 reagent (Life Technologies) and G418 resistant, RFP^+ clones were expanded. Viral transduction was done as previously described (Koo et al., 2012) using a pLV lentivirus containing a CMV-promoter-H2B-Dendra2-IRES-puro cassette and maintained under continuous puromycin selection to assure transgene expression.

RT-PCR analysis. DNase-treated RNA was used for RT-PCR analysis as previously described (Farin et al., 2012). For a list of primers used see Table S1.

Caco-2 and HT-29 cells were grown in adherent culture in DMEM supplemented with 10% fetal bovine serum, penicillin/streptomycin, and 1X Glutamax (Life Technologies) and stimulated at 70% confluence.

Lysozyme quantification and Western blotting. Organoids were collected in cold medium and sheared by pipetting to generate epithelial fragments that were subsequently washed twice in ice-cold medium to separate cells from debris and lysozyme was secreted into the crypt lumen. Cells were lysed using RIPA buffer (50 mM Tris-HCl, pH 8.0, 150 mM NaCl, 0.1% SDS, 0.5% Na-Deoxycholate, and 1% NP-40) containing Complete protease and phosphatase inhibitors (Roche). Protein content was quantified using standard Bradford assay. 10 µg of protein was run on a 14% SDS page and eventually transferred to a PVDF membrane and probed with rabbit anti-lysozyme (Dako; 1:10,000 in TBS-T 5% milk) and for normalization mouse anti–α-tubulin (Sigma-Aldrich; 1:3,000). After washes, membranes were incubated with secondary HRP-conjugated antibodies (goat anti–rabbit HRP 1:20,000 and rabbit anti–mouse 1:6,000; GE healthcare) and exposed to x-ray films using ECL reagents (GE Healthcare) and signals were quantified using ImageJ software (National Institutes of Health).

Organoid stainings, live microscopy, and transmission electron microscopy. Whole-mount immunofluorescence and immunohistochemistry, histological stainings and in situ hybridization on formalin fixed paraffin sections organoids were performed as previously described (Farin et al., 2012). Antibodies used were rabbit anti-lysozyme (Dako; 1:500) and rabbit anti-cleaved Caspase-3 (Cell Signaling Technology; 1:400). For lectin staining, organoids were fixed in Matrigel (2% PFA; o/n at 4°C). After permeabilization (0.2% Triton X-100) organoids were stained by addition of FITC-coupled *Ulex europaeus* lectin (UAE-1-FITC; Sigma-Aldrich; 5 µg/ml, 1 h at room temperature), washed, and documented on an EVOS *fl* inverse fluorescence microscope (Advanced Microscopy Group). For membrane stainings, organoids were collected in cold medium and incubated (unfixed) with PE-conjugated monoclonal antibodies anti-CD24 (clone M1/69) and FITC-conjugated anti-MHC class II (clone M5/114.15.2; both from eBioscience at 1 µg/ml final concentration) for 1 h on ice, after washes, and documentation on an EVOS *fl* microscope.

For live imaging, organoids were seeded on glass-bottom plates in drops of 50% Matrigel/50% medium to facilitate dye penetration. After 3 d of culture, PC granules were labeled by addition 10 µM ZP-1 (Santa Cruz Biotechnology) to the culture medium for 16 h before the cultures were washed twice with CO_2-equilibrated warm medium and transferred to the culture chamber (37°C; 5% CO_2; 20% O_2) of a Leica SP5 confocal microscope. Images were acquired at 15-min intervals using low laser power. BAC transgenic organoids were imaged (as above) in 30-min intervals using 10-µm z-steps. Individual PCs were tracked using LAS software (Leica) and scored as degranulated if the red signal was <50% of the starting level. For each condition, >100 random PCs were tracked that were clearly positive for both reporters.

Transmission electron microscopy was done as described previously (Sato et al., 2009).

Flow cytometry. Organoids were collected in in TrypLE solution (Life Technologies) and single-cell suspensions were obtained after 2 cycles of mechanical break-up (using narrow-tipped pulled glass Pasteur pipettes) and incubation at 37°C (5 min). Cells were washed twice in PBS 1% BSA, and resuspended at room temperature in 500 µl PBS with 1% BSA and 2,000 U/ml DNaseI (Roche). Cells were fixed by addition of an equal volume of 4% paraformaldehyde (in PBS) for 15 min at room temperature, before washing, permeabilization using 0.1% Triton X-100, and antibody incubation (all in PBS 1% BSA) using rabbit anti-cleaved Caspase-3 (as in the previous section; 1:20 dilution; 1 h at room temperature). After washes, cells were incubated with Alexa Fluor 488–coupled secondary antibody (Molecular Probes; 1:200 dilution; 30 min at room temperature) before washes, filtering, and measurement on a FACSCalibur (BD). Single cells were gated using FSC and SSC parameters (Fig. S1 A). For anti-CD24 FACS (Fig. S1 B), dissociated, unfixed cells were incubated with FITC-conjugated anti-CD24 antibody (clone M1/69; final concentration 0.2 µg/ml; 1 h on ice). Dead cells were excluded after 7-AAD staining.

iNKT-conditioned medium. HeLa cells with or without stable overexpression of hCD1D were grown in DMEM supplemented with 10% heat-inactivated bovine calf serum, 1X Glutamax, 1X penicillin/streptomycin (all from Life Technologies) and incubated with 100 ng/ml α-GC for 24 h. Subsequently, iNKT DN32.D3 hybridoma cells (Bendelac et al., 1995) were incubated with HeLa and HeLa-CD1D cells for another 24 h in serum-free advanced DMEM/F12 medium supplemented with 1X L-Glutamine, 1X penicillin/streptomycin (Life Technologies), and rhIL-2 (10 U/ml; Proleukin; Novartis). SNs were centrifuged for cell depletion and included into the regular organoid medium as 40% (vol/vol). IFN-γ levels were measured with a commercially available Elisa kit from BD. A standard curve was recorded using recombinant mouse IFN-γ protein. In some experiments, SNs were treated with functional grade anti–mouse IFN-γ monoclonal (clone XMG1.2) or rat IgG1 K isotype control (clone eBRG1; both from eBioscience; final concentrations 0.5 µg/ml) 30 min before addition to the organoids.

Mouse experiments and anti-CD3 injections. Experiments were performed according to guidelines and reviewed by the Dier Experimenten Commissie (DEC) of the KNAW. *IFN-γ* knockout (Dalton et al., 1993) and background/sex/age matched wild-type C57BL/6 mice were obtained from The Jackson Laboratory. 8-wk-old wild-type and knockout mice were injected i.p. with functional grade anti–mouse CD3e antibody (50 µg per animal; clone 145-2C11; eBioscience), or carrier alone (PBS). Mice were sacrificed 24 h after injection and the intestine was processed for histology as described (van Es et al., 2005). On 4-µm sections of lysozyme, *Defa6* and anti-cleaved Caspase-3$^+$ cells were counted. In each segment of the intestine, 3 × 15 adjacent crypts were examined (45 crypts/animal/segment).

Online supplemental material. Fig. 1 shows FACS sorting of organoid cells using intracellular anti-cleaved Caspase-3 staining and anti-CD24 membrane staining. Videos 1-3 show time-lapse analysis of PC degranulation after IFN-g exposure using Zinpyr-1 staining. Videos 4 and 5 show time-lapse visualization of PC extrusion after IFN-g exposure using transgenic reporter organoid lines. Table S1 shows primer sequences used for RT-PCR analysis. Online supplemental material is available at http://www.jem.org/cgi/content/full/jem.20130753/DC1.

We want to thank Maaike van den Born, Harry Begthel, Jeroen Korving, Stieneke van den Brink, and Karien Hamer for technical assistance and Bon-Kyoung Koo for critical discussions.

H.F. Farin was supported by an EMBO long-term fellowship ALTF 706-2009. W.R. Karthaus was supported by EU/TORNADO-KBBE-222720. G. Schwank was supported by the SNF fellowship for advanced researchers PA00P3 139732 and the Human Frontiers in Science Program long-term fellowship LT000422/2012.

H. Clevers is an inventor of several patents involving the organoid culture system. The remaining authors disclose no competing financial conflicts.

Submitted: 11 April 2013
Accepted: 9 May 2014

REFERENCES

Adolph, T.E., M.F. Tomczak, L. Niederreiter, H.-J. Ko, J. Böck, E. Martinez-Naves, J.N. Glickman, M. Tschurtschenthaler, J. Hartwig, S. Hosomi, et al. 2013. Paneth cells as a site of origin for intestinal inflammation. *Nature*. 503:272–276.

Alex, P., N.C. Zachos, T. Nguyen, L. Gonzales, T.-E. Chen, L.S. Conklin, M. Centola, and X. Li. 2009. Distinct cytokine patterns identified from multiplex profiles of murine DSS and TNBS-induced colitis. *Inflamm. Bowel Dis.* 15:341–352. http://dx.doi.org/10.1002/ibd.20753

Ayabe, T., D.P. Satchell, C.L. Wilson, W.C. Parks, M.E. Selsted, and A.J. Ouellette. 2000. Secretion of microbicidal alpha-defensins by intestinal Paneth cells in response to bacteria. *Nat. Immunol.* 1:113–118. http://dx.doi.org/10.1038/77783

Barrett, J.C., S. Hansoul, D.L. Nicolae, J.H. Cho, R.H. Duerr, J.D. Rioux, S.R. Brant, M.S. Silverberg, K.D. Taylor, M.M. Barmada, et al; NIDDK IBD Genetics Consortium; Belgian-French IBD Consortium; Wellcome Trust Case Control Consortium. 2008. Genome-wide association defines more than 30 distinct susceptibility loci for Crohn's disease. *Nat. Genet.* 40:955–962. http://dx.doi.org/10.1038/ng.175

Bendelac, A., O. Lantz, M.E. Quimby, J.W. Yewdell, J.R. Bennink, and R.R. Brutkiewicz. 1995. CD1 recognition by mouse NK1+ T lymphocytes. *Science.* 268:863–865. http://dx.doi.org/10.1126/science.7538697

Bialecki, E., C. Paget, J. Fontaine, M. Capron, F. Trottein, and C. Faveeuw. 2009. Role of marginal zone B lymphocytes in invariant NKT cell activation. *J. Immunol.* 182:6105–6113. http://dx.doi.org/10.4049/jimmunol.0802273

Brandl, K., G. Plitas, B. Schnabl, R.P. DeMatteo, and E.G. Pamer. 2007. MyD88-mediated signals induce the bactericidal lectin RegIII gamma and protect mice against intestinal Listeria monocytogenes infection. *J. Exp. Med.* 204:1891–1900. http://dx.doi.org/10.1084/jem.20070563

Brinkmann, V., U. Reichard, C. Goosmann, B. Fauler, Y. Uhlemann, D.S. Weiss, Y. Weinrauch, and A. Zychlinsky. 2004. Neutrophil extracellular traps kill bacteria. *Science.* 303:1532–1535. http://dx.doi.org/10.1126/science.1092385

Cadwell, K., J.Y. Liu, S.L. Brown, H. Miyoshi, J. Loh, J.K. Lennerz, C. Kishi, W. Kc, J.A. Carrero, S. Hunt, et al. 2008. A key role for autophagy and the autophagy gene Atg16l1 in mouse and human intestinal Paneth cells. *Nature.* 456:259–263. http://dx.doi.org/10.1038/nature07416

Cadwell, K., K.K. Patel, N.S. Maloney, T.-C. Liu, A.C. Ng, C.E. Storer, R.D. Head, R. Xavier, T.S. Stappenbeck, and H.W. Virgin. 2010. Virus-plus-susceptibility gene interaction determines Crohn's disease gene Atg16L1 phenotypes in intestine. *Cell.* 141:1135–1145. http://dx.doi.org/10.1016/j.cell.2010.05.009

Cheroutre, H., F. Lambolez, and D. Mucida. 2011. The light and dark sides of intestinal intraepithelial lymphocytes. *Nat. Rev. Immunol.* 11:445–456. http://dx.doi.org/10.1038/nri3007

Chu, H., M. Pazgier, G. Jung, S.-P. Nuccio, P.A. Castillo, M.F. de Jong, M.G. Winter, S.E. Winter, J. Wehkamp, B. Shen, et al. 2012. Human α-defensin 6 promotes mucosal innate immunity through self-assembled peptide nanonets. *Science.* 337:477–481. http://dx.doi.org/10.1126/science.1218831

Clevers, H.C., and C.L. Bevins. 2013. Paneth cells: maestros of the small intestinal crypts. *Annu. Rev. Physiol.* 75:289–311. http://dx.doi.org/10.1146/annurev-physiol-030212-183744

Dalton, D.K., S. Pitts-Meek, S. Keshav, I.S. Figari, A. Bradley, and T.A. Stewart. 1993. Multiple defects of immune cell function in mice with disrupted interferon-gamma genes. *Science.* 259:1739–1742. http://dx.doi.org/10.1126/science.8456300

Di Sabatino, A., E. Miceli, W. Dhaliwal, P. Biancheri, R. Salerno, L. Cantoro, A. Vanoli, M. De Vincenzi, Cdel.V. Blanco, T.T. MacDonald, and G.R. Corazza. 2008. Distribution, proliferation, and function of Paneth cells in uncomplicated and complicated adult celiac disease. *Am. J. Clin. Pathol.* 130:34–42. http://dx.doi.org/10.1309/5ADNAR4VN11TTKQ6

Duerkop, B.A., S. Vaishnava, and L.V. Hooper. 2009. Immune responses to the microbiota at the intestinal mucosal surface. *Immunity.* 31:368–376. http://dx.doi.org/10.1016/j.immuni.2009.08.009

Eriguchi, Y., S. Takashima, H. Oka, S. Shimoji, K. Nakamura, H. Uryu, S. Shimoda, H. Iwasaki, N. Shimono, T. Ayabe, et al. 2012. Graft-versus-host disease disrupts intestinal microbial ecology by inhibiting Paneth cell production of α-defensins. *Blood.* 120:223–231. http://dx.doi.org/10.1182/blood-2011-12-401166

Farin, H.F., J.H. Van Es, and H. Clevers. 2012. Redundant sources of Wnt regulate intestinal stem cells and promote formation of Paneth cells. *Gastroenterology.* 143:1518–1529: e7. http://dx.doi.org/10.1053/j.gastro.2012.08.031

Fernandez, M.-I., B. Regnault, C. Mulet, M. Tanguy, P. Jay, P.J. Sansonetti, and T. Pédron. 2008. Maturation of paneth cells induces the refractory state of newborn mice to Shigella infection. *J. Immunol.* 180:4924–4930. http://dx.doi.org/10.4049/jimmunol.180.7.4924

Giblin, L.J., C.J. Chang, A.F. Bentley, C. Frederickson, S.J. Lippard, and C.J. Frederickson. 2006. Zinc-secreting Paneth cells studied by ZP fluorescence. *J. Histochem. Cytochem.* 54:311–316. http://dx.doi.org/10.1369/jhc.5A6724.2005

Grootjans, J., C.M. Hodin, J.-J. de Haan, J.P.M. Derikx, K.M.A. Rouschop, F.K. Verheyen, R.M. van Dam, C.H.C. Dejong, W.A. Buurman, and K. Lenaerts. 2011. Level of activation of the unfolded protein response correlates with Paneth cell apoptosis in human small intestine exposed to ischemia/reperfusion. *Gastroenterology.* 140:529–539:e3. http://dx.doi.org/10.1053/j.gastro.2010.10.040

Guy-Grand, D., J.P. DiSanto, P. Henchoz, M. Malassis-Séris, and P. Vassalli. 1998. Small bowel enteropathy: role of intraepithelial lymphocytes and of cytokines (IL-12, IFN-gamma, TNF) in the induction of epithelial cell death and renewal. *Eur. J. Immunol.* 28:730–744. http://dx.doi.org/10.1002/(SICI)1521-4141(199802)28:02<730::AID-IMMU730>3.0.CO;2-U

Ireland, H., C. Houghton, L. Howard, and D.J. Winton. 2005. Cellular inheritance of a Cre-activated reporter gene to determine Paneth cell longevity in the murine small intestine. *Dev. Dyn.* 233:1332–1336. http://dx.doi.org/10.1002/dvdy.20446

Kaser, A., A.-H. Lee, A. Franke, J.N. Glickman, S. Zeissig, H. Tilg, E.E.S. Nieuwenhuis, D.E. Higgins, S. Schreiber, L.H. Glimcher, and R.S. Blumberg. 2008. XBP1 links ER stress to intestinal inflammation and confers genetic risk for human inflammatory bowel disease. *Cell.* 134:743–756. http://dx.doi.org/10.1016/j.cell.2008.07.021

Kobayashi, K.S., M. Chamaillard, Y. Ogura, O. Henegariu, N. Inohara, G. Nuñez, and R.A. Flavell. 2005. Nod2-dependent regulation of innate and adaptive immunity in the intestinal tract. *Science.* 307:731–734. http://dx.doi.org/10.1126/science.1104911

Kontoyiannis, D., G. Boulougouris, M. Manoloukos, M. Armaka, M. Apostolaki, T. Pizarro, A. Kotlyarov, I. Forster, R. Flavell, M. Gaestel, et al. 2002. Genetic dissection of the cellular pathways and signaling mechanisms in modeled tumor necrosis factor-induced Crohn's-like inflammatory bowel disease. *J. Exp. Med.* 196:1563–1574. http://dx.doi.org/10.1084/jem.20020281

Koo, B.-K., D.E. Stange, T. Sato, W. Karthaus, H.F. Farin, M. Huch, J.H. van Es, and H. Clevers. 2012. Controlled gene expression in primary Lgr5 organoid cultures. *Nat. Methods.* 9:81–83. http://dx.doi.org/10.1038/nmeth.1802

Lee, H.T., M. Kim, J.Y. Kim, K.M. Brown, A. Ham, V.D. D'Agati, and Y. Mori-Akiyama. 2013. Critical role of interleukin-17A in murine intestinal ischemia-reperfusion injury. *Am. J. Physiol. Gastrointest. Liver Physiol.* 304:G12–G25. http://dx.doi.org/10.1152/ajpgi.00201.2012

Levine, J.E., E. Huber, S.T.G. Hammer, A.C. Harris, J.K. Greenson, T.M. Braun, J.L.M. Ferrara, and E. Holler. 2013. Low Paneth cell numbers at onset of gastrointestinal graft-versus-host disease identify patients at high risk for nonrelapse mortality. *Blood.* 122:1505–1509. http://dx.doi.org/10.1182/blood-2013-02-485813

Lotz, M., D. Gütle, S. Walther, S. Ménard, C. Bogdan, and M.W. Hornef. 2006. Postnatal acquisition of endotoxin tolerance in intestinal epithelial cells. *J. Exp. Med.* 203:973–984. http://dx.doi.org/10.1084/jem.20050625

Merger, M., J.L. Viney, R. Borojevic, D. Steele-Norwood, P. Zhou, D.A. Clark, R. Riddell, R. Maric, E.R. Podack, and K. Croitoru. 2002. Defining the roles of perforin, Fas/FasL, and tumour necrosis factor alpha in T cell induced mucosal damage in the mouse intestine. *Gut.* 51:155–163. http://dx.doi.org/10.1136/gut.51.2.155

Meyer-Hoffert, U., M.W. Hornef, B. Henriques-Normark, L.-G. Axelsson, T. Midtvedt, K. Pütsep, and M. Andersson. 2008. Secreted enteric antimicrobial activity localises to the mucus surface layer. *Gut.* 57:764–771. http://dx.doi.org/10.1136/gut.2007.141481

Miura, N., M. Yamamoto, M. Fukutake, N. Ohtake, S. Iizuka, A. Ishige, H. Sasaki, K. Fukuda, T. Yamamoto, and S. Hayakawa. 2005. Anti-CD3 induces bi-phasic apoptosis in murine intestinal epithelial cells: possible involvement of the Fas/Fas ligand system in different T cell compartments. *Int. Immunol.* 17:513–522. http://dx.doi.org/10.1093/intimm/dxh231

Mukherjee, S., S. Vaishnava, and L.V. Hooper. 2008. Multi-layered regulation of intestinal antimicrobial defense. *Cell. Mol. Life Sci.* 65:3019–3027. http://dx.doi.org/10.1007/s00018-008-8182-3

Nieuwenhuis, E.E., T. Matsumoto, M. Exley, R.A. Schleipman, J. Glickman, D.T. Bailey, N. Corazza, S.P. Colgan, A.B. Onderdonk, and R.S. Blumberg. 2002. CD1d-dependent macrophage-mediated clearance of Pseudomonas aeruginosa from lung. *Nat. Med.* 8:588–593. http://dx.doi.org/10.1038/nm0602-588

Nieuwenhuis, E.E., T. Matsumoto, D. Lindenbergh, R. Willemsen, A. Kaser, Y. Simons-Oosterhuis, S. Brugman, K. Yamaguchi, H. Ishikawa, Y. Aiba, et al. 2009. Cd1d-dependent regulation of bacterial colonization in the intestine of mice. *J. Clin. Invest.* 119:1241–1250. http://dx.doi.org/10.1172/JCI36509

Nilsen, E.M., F.L. Jahnsen, K.E. Lundin, F.E. Johansen, O. Fausa, L.M. Sollid, J. Jahnsen, H. Scott, and P. Brandtzaeg. 1998. Gluten induces an intestinal cytokine response strongly dominated by interferon gamma in patients with celiac disease. *Gastroenterology*. 115:551–563. http://dx.doi.org/10.1016/S0016-5085(98)70134-9

Raetz, M., S.H. Hwang, C.L. Wilhelm, D. Kirkland, A. Benson, C.R. Sturge, J. Mirpuri, S. Vaishnava, B. Hou, A.L. Defranco, et al. 2013. Parasite-induced TH1 cells and intestinal dysbiosis cooperate in IFN-γ-dependent elimination of Paneth cells. *Nat. Immunol.* 14:136–142. http://dx.doi.org/10.1038/ni.2508

Rumio, C., M. Sommariva, L. Sfondrini, M. Palazzo, D. Morelli, L. Viganò, L. De Cecco, E. Tagliabue, and A. Balsari. 2012. Induction of Paneth cell degranulation by orally administered Toll-like receptor ligands. *J. Cell. Physiol.* 227:1107–1113. http://dx.doi.org/10.1002/jcp.22830

Saha, S., X. Jing, S.Y. Park, S. Wang, X. Li, D. Gupta, and R. Dziarski. 2010. Peptidoglycan recognition proteins protect mice from experimental colitis by promoting normal gut flora and preventing induction of interferon-γ. *Cell Host Microbe*. 8:147–162. http://dx.doi.org/10.1016/j.chom.2010.07.005

Salzman, N.H., K. Hung, D. Haribhai, H. Chu, J. Karlsson-Sjöberg, E. Amir, P. Teggatz, M. Barman, M. Hayward, D. Eastwood, et al. 2010. Enteric defensins are essential regulators of intestinal microbial ecology. *Nat. Immunol.* 11:76–83. http://dx.doi.org/10.1038/ni.1825

Sato, T., R.G. Vries, H.J. Snippert, M. van de Wetering, N. Barker, D.E. Stange, J.H. van Es, A. Abo, P. Kujala, P.J. Peters, and H. Clevers. 2009. Single Lgr5 stem cells build crypt-villus structures in vitro without a mesenchymal niche. *Nature*. 459:262–265. http://dx.doi.org/10.1038/nature07935

Sato, T., J.H. van Es, H.J. Snippert, D.E. Stange, R.G. Vries, M. van den Born, N. Barker, N.F. Shroyer, M. van de Wetering, and H. Clevers. 2011a. Paneth cells constitute the niche for Lgr5 stem cells in intestinal crypts. *Nature*. 469:415–418. http://dx.doi.org/10.1038/nature09637

Sato, T., D.E. Stange, M. Ferrante, R.G.J. Vries, J.H. Van Es, S. Van den Brink, W.J. Van Houdt, A. Pronk, J. Van Gorp, P.D. Siersema, and H. Clevers. 2011b. Long-term expansion of epithelial organoids from human colon, adenoma, adenocarcinoma, and Barrett's epithelium. *Gastroenterology*. 141:1762–1772. http://dx.doi.org/10.1053/j.gastro.2011.07.050

Satoh, Y. 1988. Atropine inhibits the degranulation of Paneth cells in exgerm-free mice. *Cell Tissue Res.* 253:397–402. http://dx.doi.org/10.1007/BF00222296

Satoh, Y., K. Ishikawa, Y. Oomori, S. Takeda, and K. Ono. 1992. Bethanechol and a G-protein activator, NaF/AlCl3, induce secretory response in Paneth cells of mouse intestine. *Cell Tissue Res.* 269:213–220. http://dx.doi.org/10.1007/BF00319611

Sawada, M., K. Takahashi, S. Sawada, and O. Midorikawa. 1991. Selective killing of Paneth cells by intravenous administration of dithizone in rats. *Int. J. Exp. Pathol.* 72:407–421.

Schwank, G., A. Andersson-Rolf, B.-K. Koo, N. Sasaki, and H. Clevers. 2013. Generation of BAC transgenic epithelial organoids. *PLoS ONE*. 8:e76871. http://dx.doi.org/10.1371/journal.pone.0076871

Tanabe, H., T. Ayabe, B. Bainbridge, T. Guina, R.K. Ernst, R.P. Darveau, S.I. Miller, and A.J. Ouellette. 2005. Mouse paneth cell secretory responses to cell surface glycolipids of virulent and attenuated pathogenic bacteria. *Infect. Immun.* 73:2312–2320. http://dx.doi.org/10.1128/IAI.73.4.2312-2320.2005

Tewary, P., G. de la Rosa, N. Sharma, L.G. Rodriguez, S.G. Tarasov, O.M.Z. Howard, H. Shirota, F. Steinhagen, D.M. Klinman, D. Yang, and J.J. Oppenheim. 2013. β-Defensin 2 and 3 promote the uptake of self or CpG DNA, enhance IFN-α production by human plasmacytoid dendritic cells, and promote inflammation. *J. Immunol.* 191:865–874. http://dx.doi.org/10.4049/jimmunol.1201648

Vaishnava, S., C.L. Behrendt, A.S. Ismail, L. Eckmann, and L.V. Hooper. 2008. Paneth cells directly sense gut commensals and maintain homeostasis at the intestinal host-microbial interface. *Proc. Natl. Acad. Sci. USA*. 105:20858–20863. http://dx.doi.org/10.1073/pnas.0808723105

van Es, J.H., P. Jay, A. Gregorieff, M.E. van Gijn, S. Jonkheer, P. Hatzis, A. Thiele, M. van den Born, H. Begthel, T. Brabletz, et al. 2005. Wnt signalling induces maturation of Paneth cells in intestinal crypts. *Nat. Cell Biol.* 7:381–386. http://dx.doi.org/10.1038/ncb1240

van Es, J.H., T. Sato, M. van de Wetering, A. Lyubimova, A.N.Y. Nee, A. Gregorieff, N. Sasaki, L. Zeinstra, M. van den Born, J. Korving, et al. 2012. Dll1+ secretory progenitor cells revert to stem cells upon crypt damage. *Nat. Cell Biol.* 14:1099–1104. http://dx.doi.org/10.1038/ncb2581

Wehkamp, J., and E.F. Stange. 2010. Paneth's disease. *J. Crohn's Colitis*. 4:523–531. http://dx.doi.org/10.1016/j.crohns.2010.05.010

Wehkamp, J., J. Harder, M. Weichenthal, M. Schwab, E. Schäffeler, M. Schlee, K.R. Herrlinger, A. Stallmach, F. Noack, P. Fritz, et al. 2004. NOD2 (CARD15) mutations in Crohn's disease are associated with diminished mucosal alpha-defensin expression. *Gut*. 53:1658–1664. http://dx.doi.org/10.1136/gut.2003.032805

Wehkamp, J., G. Wang, I. Kübler, S. Nuding, A. Gregorieff, A. Schnabel, R.J. Kays, K. Fellermann, O. Burk, M. Schwab, et al. 2007. The Paneth cell alpha-defensin deficiency of ileal Crohn's disease is linked to Wnt/Tcf-4. *J. Immunol.* 179:3109–3118. http://dx.doi.org/10.4049/jimmunol.179.5.3109

Wilson, C.L., A.J. Ouellette, D.P. Satchell, T. Ayabe, Y.S. López-Boado, J.L. Stratman, S.J. Hultgren, L.M. Matrisian, and W.C. Parks. 1999. Regulation of intestinal alpha-defensin activation by the metalloproteinase matrilysin in innate host defense. *Science*. 286:113–117. http://dx.doi.org/10.1126/science.286.5437.113

Zhao, F., R. Edwards, D. Dizon, K. Afrasiabi, J.R. Mastroianni, M. Geyfman, A.J. Ouellette, B. Andersen, and S.M. Lipkin. 2010. Disruption of Paneth and goblet cell homeostasis and increased endoplasmic reticulum stress in Agr2−/− mice. *Dev. Biol.* 338:270–279. http://dx.doi.org/10.1016/j.ydbio.2009.12.008